energies

MDPI

Article

Ab-Initio Molecular Dynamics Simulation of Condensed-Phase Reactivity: The Electrolysis of Ammonia and Ethanimine in Aquatic Carbon Dioxide Solutions

Igor Gordiy, Lukas Steinbach and Irmgard Frank *

Theoretische Chemie, Universität Hannover, Callinstr. 3A, 30167 Hannover, Germany; I.Gordiy@campus.lmu.de (I.G.); lukas.steinbach@stud.uni-hannover.de (L.S.)
* Correspondence: irmgard.frank@theochem.uni-hannover.de

Abstract: The re-use of wastewater is an increasingly important subject. Most recently, several attempts were reported to convert wastewater in harmless or even valuable substances by the use of electrical current. Electrochemistry is an old approach. The renewed interest stems from the fact that electrical current is often available in abundance, for example from solar energy in arid regions, while clean water is not. Experimentally, one has to deal with very many products which are the result of many reaction steps. Here, theory can help. Using Car–Parrinello molecular dynamics, we simulate the first few reaction steps of the electrolysis of wastewater. On the basis of previous studies, we investigate the reaction of carbon dioxide and nitrogen compounds. The results show a great variety of reaction steps and resulting products. Some of them are technologically interesting, such as hydrogen and formic acid.

Keywords: ab initio molecular dynamics; reaction mechanisms; electrolysis; wastewater; power-to-fuel

Citation: Gordiy, I.; Steinbach, L.; Frank, I. Ab-Initio Molecular Dynamics Simulation of Condensed-Phase Reactivity: The Electrolysis of Ammonia and Ethanimine in Aquatic Carbon Dioxide Solutions. *Energies* **2021**, *14*, 6510. https://doi.org/10.3390/en14206510

Academic Editor: Bohung Kim

Received: 30 August 2021
Accepted: 4 October 2021
Published: 11 October 2021

1. Introduction

The removal of wastewater is an industrial process in all regions of the world. The reasons for this are manifold. There are huge amounts of municipal wastewater in regions with high population density as metropolitan areas. Additionally, agricultural and industrial plants produce contaminated water in their processes [1].

One way to get rid of bioorganic and inorganic contamination in wastewater is the electrolysis of the pollutants. Thereby, different strategies are pursued. One way is the degradation of all chemicals to gaseous, harmless species like H_2, N_2, O_2 and CO_2. The second way is to produce different chemicals which contain higher energies in concepts such as "power to fuel" [2–4] and "power to gas" [5–8] or summarized as "power to chemicals" [9,10]. The electrolytic conversion of wastewater pollutants has the benefit of combining two advantages. While electrolytic reactions can lead to desired products, the degradation simultaneously taking place can lead to further synthesis routes, e.g., Fischer-Tropsch synthesis [11,12], with H_2 and CO_2. Experimentally, the number of compounds which may be generated is vast. Theoretical studies may help to find the most important intermediates and products [13]. The reactivity of biomolecules, such as peptides and urea, that are likely to be found in municipal and agricultural wastewater were studied in previous publications [14,15]. The outcomes of these studies in the picosecond timescale were solutions containing ammonia, ethanimine, and carbon dioxide which are going to be investigated in this work. For the electrolytic reaction of ammonia several mechanisms were stated in the past [16–18]. These results were mainly derived from experimental data, which focus on the products of the reaction, determined with the help of various methods.

In this work the ultra-fast reactions taking place under electrolytic conditions are investigated for their mechanism with focus on intermediate products and their energetics.

In contrast to other studies [19,20], we focus on the outer Helmholtz layer only. That is, we investigate the reactions which occur without direct contact with the surface of an electrode. Conditions at a distance from the electrode surface are simulated by creating OH or H radicals solvated in the aquatic environment of the simulation. The performance of our approach for such a system was investigated in reference [21]. In our simulations the radicals are created via simply removing nuclei and electrons from water molecules after an equilibration phase [14,15,22]. This approach models the situation immediately after the electron transfer. The electron transfer itself is not part of our simulations. Simulating this electron transfer would be difficult because our simulation boxes are small, and we use self-consistent field theory. Ionic species would be discharged by electronic tunneling already at a distance from the electrode surface. The radicals resulting from our simulations are reactive open shell molecules, which attack the molecules in the solution in different ways. The reactions are taking place in the picosecond timescale, so for investigations on the reaction mechanism, Car–Parrinello molecular dynamics (CPMD) [23–25] with up to 0.1 femtosecond timesteps can be used for the simulation. The use of the CPMD method has various advantages. CPMD describes the movement of all parts of a system in a limited timestep. This on-the-fly approach offers the advantage that reaction pathways can be found and not only known ones can be analyzed. CPMD describes the movement of both, the nuclei and the electrons of the system which leads to a good description of the reaction path and the mechanism [26]. However, the simulation of the movement of the whole molecular system leads to the disadvantage of high computing times. And as a result of these high computational efforts the strength of this molecular dynamics method causes also its limitation on a relative low number of timesteps. This makes CPMD only useful for the description of very fast reactions.

To accelerate the reactions and to observe as many reactions as possible, we use a very high density of active species. This may lead to reaction mechanisms that are not relevant under conditions that are closer to experiment. However, it is possible to monitor if, for a certain reaction, the simultaneous attack of two reactive species is needed. Hence, we must discuss in the end which reactions are overestimated due to the high number of reactive species. The products depend strongly on the initial conditions after equilibration; hence, we must perform as many simulation runs as possible.

Under such highly reactive conditions as they are to be found during electrolysis, many different reactions are taking place so that a selection which ones to discuss had to be made. For this reason, the selected reactions which are discussed in this work, was limited to stable products. The complete simulation data including the unstable open shell products can be found in the Supplementary Materials.

To limit the amount of CPU time used for the molecular dynamic simulations, we are restricted to GGA functionals such as BLYP-D3 [27–29] which has an incredible accuracy/cost relation, but also has well-known weaknesses. Hence, while the molecular dynamics runs were performed using CPMD in combination with BLYP-D3, the energetic properties of the products have been calculated with various methods as implemented in the Gaussian program code [30]. Wave-function, DFT and hybrid methods were used, further detail is given in the Methods section. The electronic energies $\Delta_r E$ and the heat of reaction $\Delta_r H$ were calculated and compared to the experiment. The complete results are summarized in the Supplementary Materials.

2. Methods

Car–Parrinello molecular dynamics simulations using the CPMD code [23] were performed using the Becke–Lee–Yang–Parr (BLYP) [31,32] functional in connection with the Grimme dispersion correction [33]. The time step was chosen as 2 a.u. (0.048 fs) and the fictitious electron mass as 200 a.u. Troullier–Martins pseudopotentials as optimized for the BLYP functional were employed for describing the core electrons [34,35]. The plane-wave cutoff, which determines the size of the basis set, was set to 70.0 Rydberg. The simulation

cells were 20 × 20 × 20 a.u.^{3} or 10.6 × 10.6 × 10.6 Å^3. For the reactive simulations, the unrestricted version of Kohn–Sham theory was employed [36,37].

The density of the created solutions is higher than that of pure water (1.00 g/cm^3) because several water molecules are substituted with CO_2, which has a higher molecular weight. Solutions with a density of roughly 1.22 g/cm^3 were generated (8 ammonia, 9 carbon dioxide and 19 water molecules named system 1 or 7 ammonia, 9 carbon dioxide and 19 water molecules named system 2). Additionally, solutions with ethanimine were generated (4 ethanimine, 9 carbon dioxide, and 21 water molecules named system 3 or 4 ethanimine, 9 carbon dioxide and 22 water molecules named system 4). The solutions of systems 3 and 4 had a density of roughly 1.34 g/cm^3. After the equilibration of stable, neutral, closed-shell systems, reactive species were generated in two ways: by removing eight hydrogen radicals, leading to OH radicals in order to simulate anodic conditions and by removing eight OH radicals, leading to eight hydrogen radicals in order to simulate cathodic conditions. For the reactive simulations, the spin-unrestricted version of Kohn–Sham theory was employed. To check the radical character of the observed species, we computed Mulliken charges.

The geometry optimizations were performed with the Gaussian 16 program package [30]. All geometry optimizations and vibrational frequency calculations were performed using the BLYP-D3 [31–33] functional, the B3LYP-D3 [38,39] hybrid functional, the B2PLYP-D3 [39] double hybrid functional, the Hartree–Fock method, the second order Møller–Plesset perturbation method MP2 [40], and the coupled cluster CCSD method in combination with the 6-311G(d,p) basis set [41]. Additionally, further calculations were performed using the CCSD method with the aug-cc-pVTZ basis set which will be referred to as CCSD/aug. In all calculations solvent effects for water were taken into account with the PCM continuum solvation model [42]. The thermodynamic data were calculated using the freq keyword function of the Gaussian 16 program.

3. Results and Discussion

The most complex and important processes were observed during simulations of anodic conditions, that is why it makes more sense to begin the discussion with their detailed description. In order to better simulate the real systems, two new cells were created for each neutral equilibrated system, which differed only in the positions of created OH radicals. As expected, the formation of various reactive oxygen-based species was observed (e.g., hydrogen peroxide HOOH, HOO radical, O_2). Furthermore, ammonia molecules were oxidized to several inorganic compounds, such as NHO, NO, NH_2OH, NH_2O, and NH_2. Furthermore, ethanimine molecules were oxidized to several organic compounds, such as RNHO, nitrene radical, RNO radical, oxime. R is equal to ethylidene group.

3.1. Ammonia and Carbon Dioxide in Aqueous Solution

3.1.1. Anodic Reactions

The first reaction observed is the formation of an HNO molecule out of NH_3. The mechanism is shown in Figure 1.

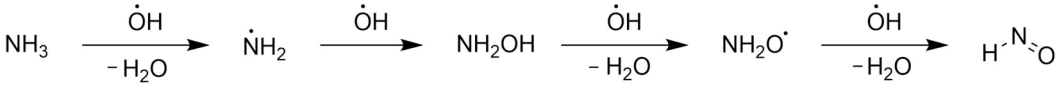

Figure 1. Sequence of elementary reaction steps that lead to the formation of HNO molecule in system 1. The initial temperature of the system was set to 250 K.

Its first reaction step corresponds to the abstraction of hydrogen radical from ammonia by OH radical which results in the formation of NH_2 radical after 0.16 ps of simulation. The formed reactive intermediate is attacked further by a second OH radical within 0.02 ps. As a result, the stable closed-shell hydroxylamine molecule is formed. Key bond lengths for first and second reaction steps are depicted in Figure 2. Afterwards the hydrogen atom

of the hydroxyl group is attacked by a third OH radical which results in the formation of an NH_2O radical and a water molecule. The new reactive intermediate is stabilized during the last step of the reaction via hydrogen radical abstraction, which is performed by the fourth OH radical. The closed-shell stable HNO molecule is formed after 0.35 ps. Key bond lengths for the third and fourth reaction steps are depicted in Figures 3 and 4.

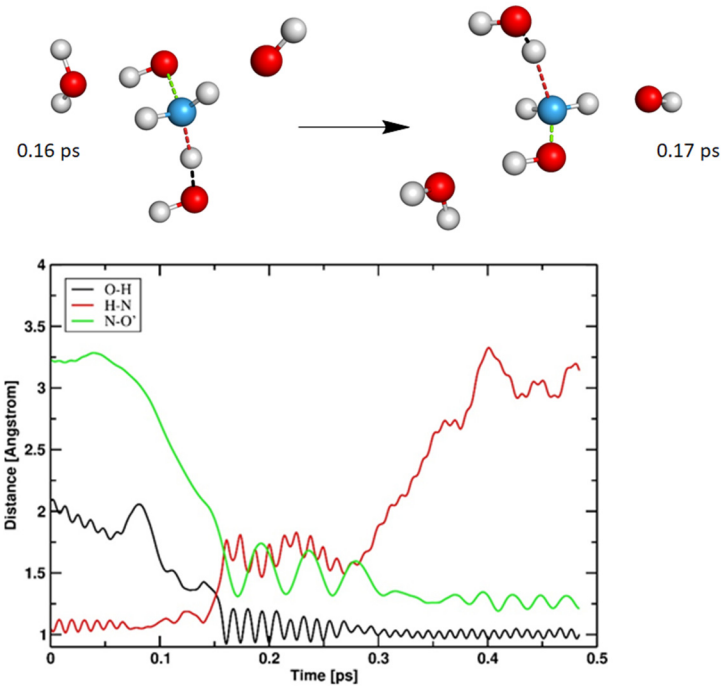

Figure 2. Sketch of the first and second reaction steps of ammonia with OH radicals observed for system 1. The most relevant bonding interactions deduced from Car–Parrinello simulations are highlighted. An extremely short-lived intermediate can be identified in the time regime 0.15–0.30 ps. Both the N-H and the O-H bonds are oscillating at the length of a hydrogen bridge. Color-code: blue—nitrogen, red—oxygen; white—hydrogen.

Among the reactions observed another mechanism for the formation of HNO was found for system 2, and it is depicted in Figure 5.

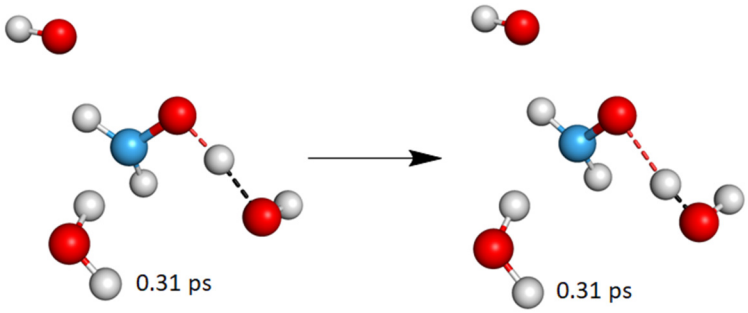

Figure 3. *Cont.*

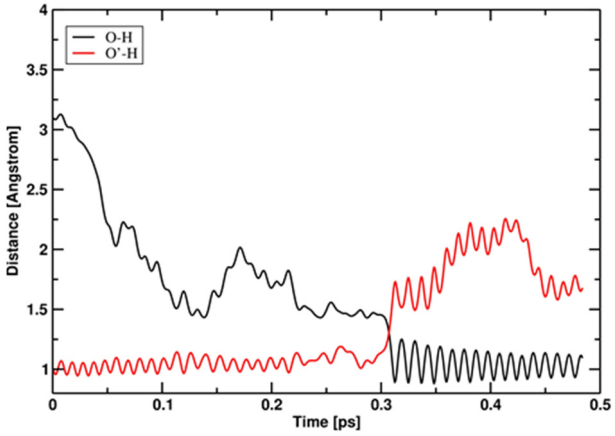

Figure 3. Sketch of the third reaction step observed for system 1. Reaction of hydroxylamine with OH radical. The most relevant bonding interactions deduced from Car–Parrinello simulations are highlighted. The abstraction of a hydrogen atom from the OH group of the hydroxylamine molecule can be observed. In the same step water is formed, stabilizing the formed radical. Color-code: blue—nitrogen, red—oxygen; white—hydrogen.

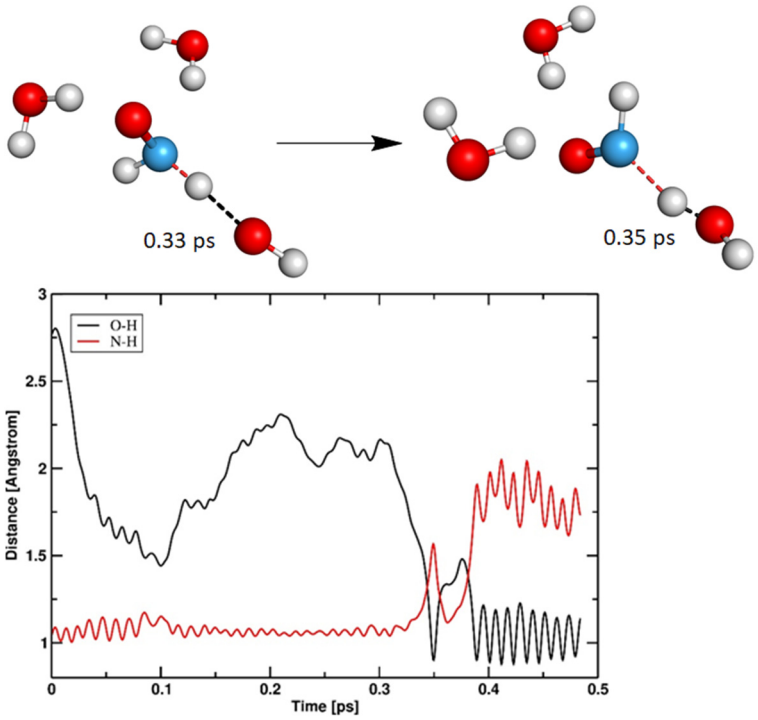

Figure 4. Sketch of the fourth reaction step observed for system 1. NH_2O radical reacts with OH radical and eliminates water. The most relevant bonding interactions deduced from Car–Parrinello simulations are highlighted. Color-code: blue—nitrogen, red—oxygen; white—hydrogen.

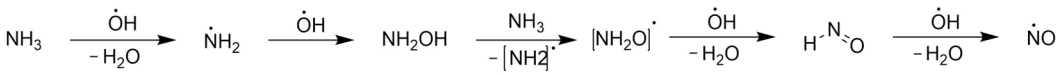

Figure 5. Sequence of elementary reaction steps that lead to the formation of an NHO molecule in system 2. The initial temperature was set to 300 K.

The first reaction step corresponds to the attack of a hydroxyl radical on ammonia, which results in the formation of an NH_3OH radical after 0.15 ps of simulation. The formed

reactive and very unstable intermediate is attacked further by a second OH radical within less than 0.01 ps resulting in the formation of the closed-shell NH_2OH product and a water molecule. Key bond lengths for the first and second reaction steps are depicted in Figure 6. During the third step the highly reactive hydroxylamine reacts with a second NH_3 molecule yielding the NH_2O radical intermediate and a neutral ammonium radical after 0.02 ps. The reaction step is depicted in Figure 7. The last step is the attack of a hydroxyl radical, which abstracts a hydrogen radical yielding a stable closed-shell NHO molecule and water. The reaction is completed within 0.39 ps. Key bond lengths for the fourth reaction step are depicted in Figure 8.

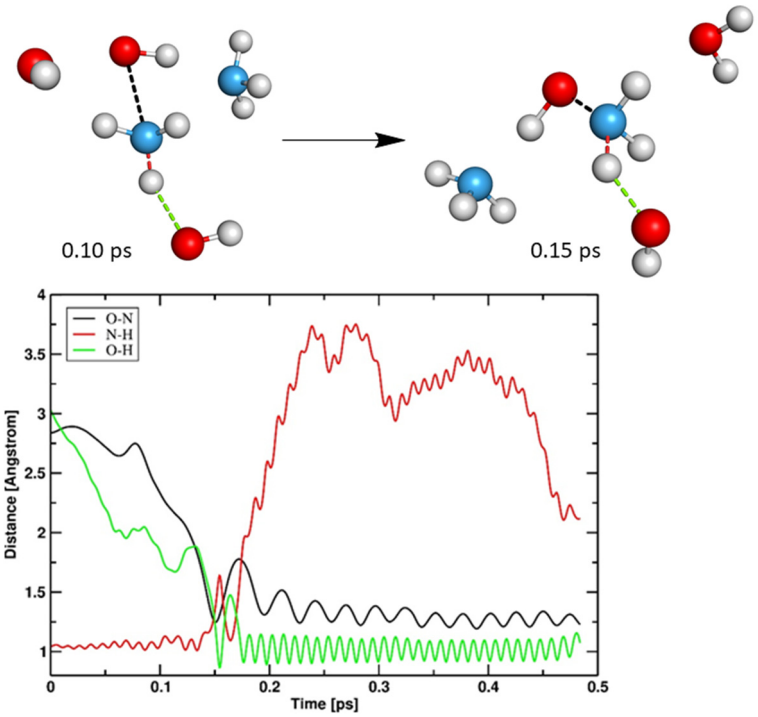

Figure 6. Sketch of the first and second reaction step (system 2). In the first step ammonia is attacked by an OH radical which leads to the formation of an NH_3OH radical. In the second step, almost simultaneously, another OH radical is attacking, leading to the elimination of water and the formation of hydroxylamine. Color-code: blue—nitrogen, red—oxygen; white—hydrogen.

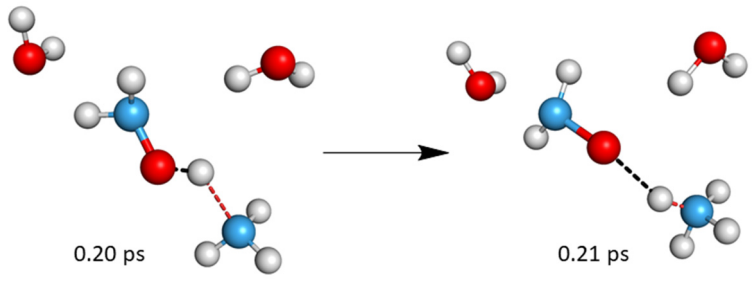

Figure 7. *Cont.*

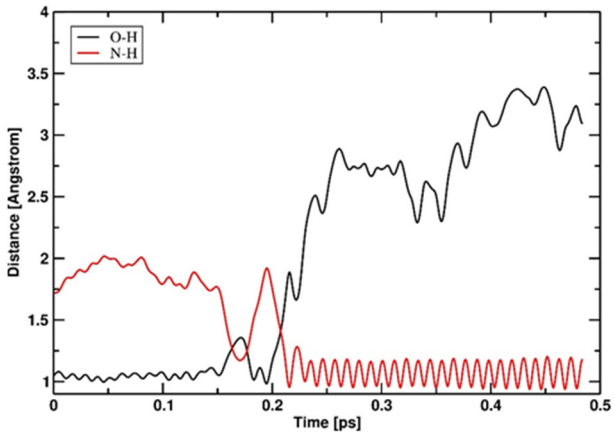

Figure 7. Sketch of the third reaction step (system 2). The hydroxylamine molecule is attacked by ammonia, leading to the formation of an NH_2O-radical and a NH_4 radical. Color-code: blue—nitrogen, red—oxygen; white—hydrogen.

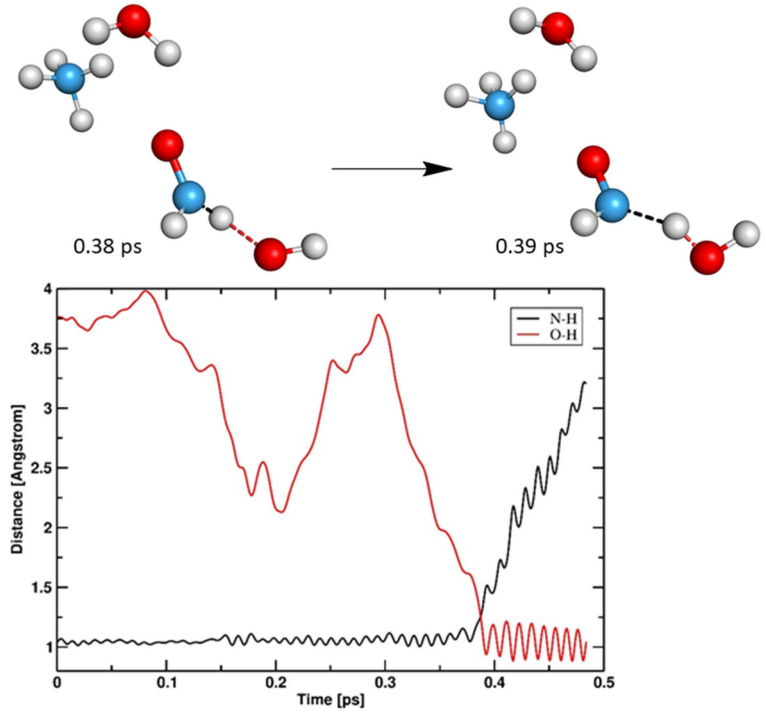

Figure 8. Sketch of the fourth reaction step (system 2). The attack of another OH radical on the NH_2O radical and the following elimination of water leads to the formation of the closed-shell HNO molecule. Color-code: blue—nitrogen, red—oxygen; white—hydrogen.

Another reaction observed for system 1 is the formation of NO out of NH_3 with HNO as intermediate product, as depicted in Figure 9.

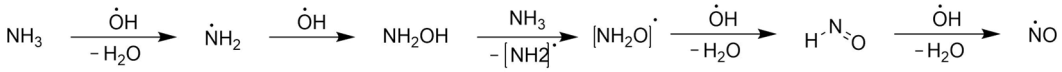

Figure 9. Second sequence of elementary reaction steps that lead to the formation of an NO molecule in a second simulation run for system 1. The initial temperature was set to 250 K.

The first reaction step corresponds to the abstraction of hydrogen radical from ammonia by an OH radical which results in the formation of an NH_2 radical after 0.06 ps of

simulation. The formed reactive intermediate is attacked further by a second OH radical within 0.05 ps resulting in the formation of the NH_2OH intermediate. Key bond lengths for the first and second reaction steps are depicted in Figure 10. During the third step hydroxyl amine reacts with a second NH_3 molecule yielding an NH_2O radical intermediate and a neutral ammonium radical after 0.14 ps of simulation. The NH_2O radical reacts further with an OH radical resulting in the formation of a water molecule and closed-shell HNO The last step is represented by the attack of a third OH radical on formerly formed HNO, which yields NO and a water molecule. The reaction is completed within 0.20 ps. Key bond lengths for the third and fourth reaction steps are depicted in Figures 11 and 12 and for the last step in Figure 13.

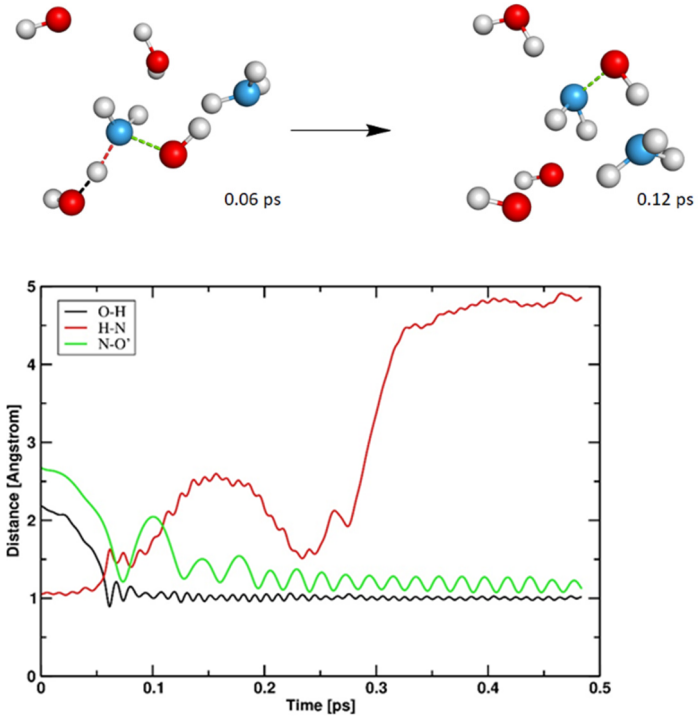

Figure 10. Sketch of the first and second reaction steps of ammonia with OH radicals. The most relevant bonding interactions deduced from Car–Parrinello simulations are highlighted. Color-code: blue—nitrogen, red—oxygen; white—hydrogen.

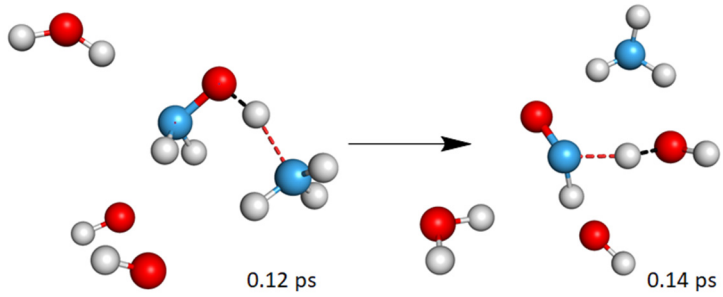

Figure 11. *Cont.*

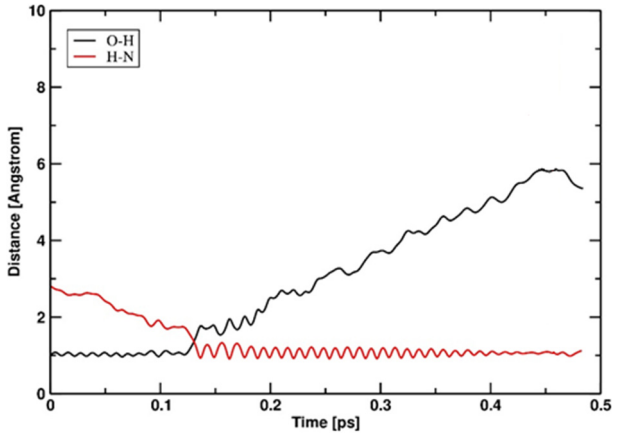

Figure 11. Sketch of the third reaction step of the formed hydroxylamine which is attacked by ammonia leading to a NH_2O radical. The most relevant bonding interactions deduced from Car–Parrinello simulations are highlighted. Color-code: blue—nitrogen, red—oxygen; white—hydrogen.

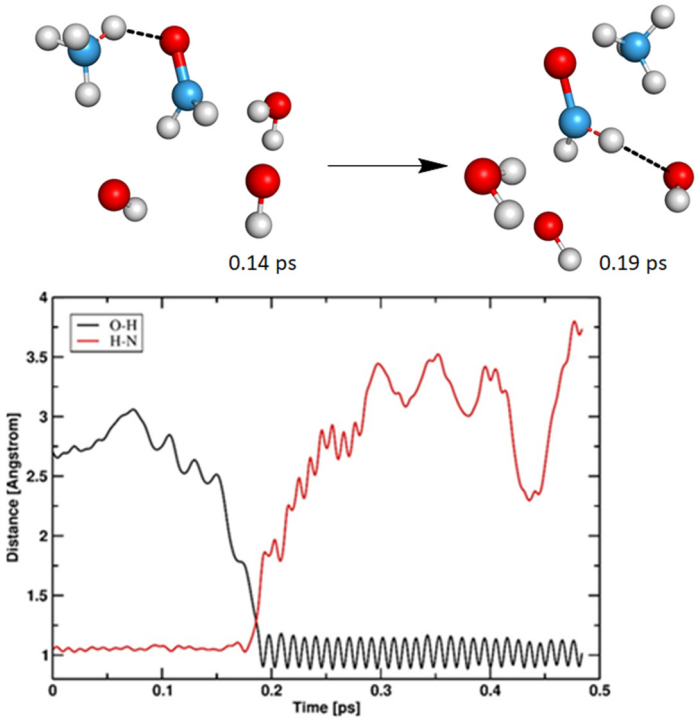

Figure 12. Sketch of the fourth reaction step of formerly formed NH_2O radical molecule with OH radical. The most relevant bonding interactions deduced from Car-Parrinello simulations are highlighted. Color-code: blue—nitrogen, red—oxygen; white—hydrogen.

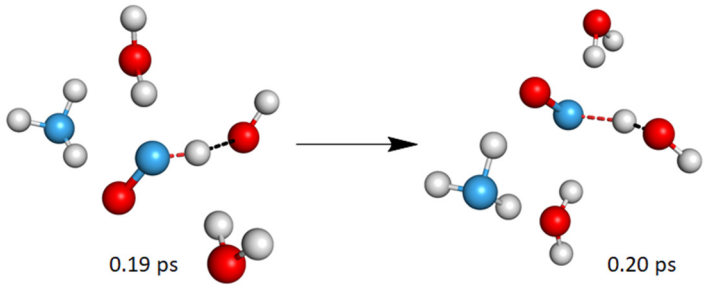

Figure 13. *Cont.*

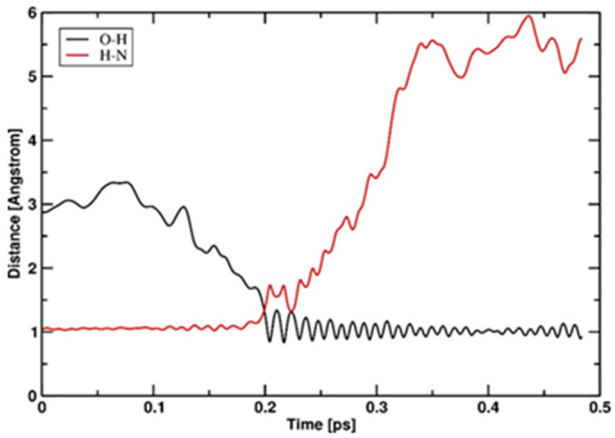

Figure 13. Sketch of the fifth reaction step of HNO with OH radical leading to the formation of an NO radical. The most relevant bonding interactions deduced from Car–Parrinello simulations are highlighted. Color-code: blue—nitrogen, red—oxygen; white—hydrogen.

In addition to HNO and NO, hydroxylamine NH_2OH is formed during the simulation of reactions in system 2, depicted in Figure 14 hydroxylamine is also an intermediate of the mechanism shown in Figure 9.

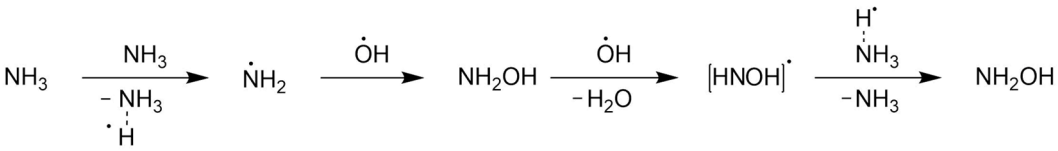

Figure 14. Sequence of elementary reaction steps that lead to the formation of NH_2OH molecule in system 2. The initial temperature was set to 300 K.

The first reaction step of the first mechanism corresponds to the homolytic dissociation of the N-H bond, which results in the formation of NH_2 and H radicals after 0.15 ps of simulation. The formed hydrogen radical is coordinated by a second equivalent of ammonia. To be more specific, a hydrogen atom is located between two nitrogen centers. The second step is represented by the recombination of OH radical with NH_2 yielding closed shell hydroxyl amine within 0.04 ps. The key bond lengths for the first and second reaction steps are depicted in Figure 15. During the third step hydroxyl amine reacts with a second OH radical yielding an HNOH radical intermediate and a water molecule after 0.01 ps. The last step is the recombination of NHOH radical with H radical and simultaneous loss of coordination by a second equivalent of ammonia, which leads to the formation of stable closed-shell hydroxylamine. The reaction is completed within 0.23 ps. Key bond lengths for the third and fourth reaction steps are depicted in Figure 16.

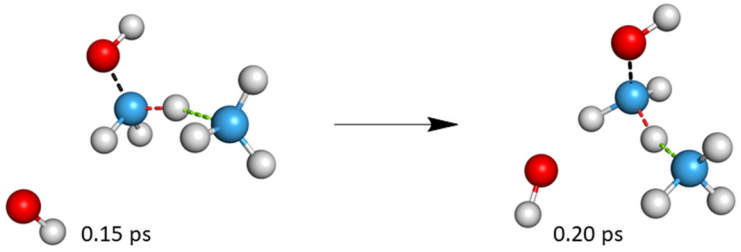

Figure 15. *Cont.*

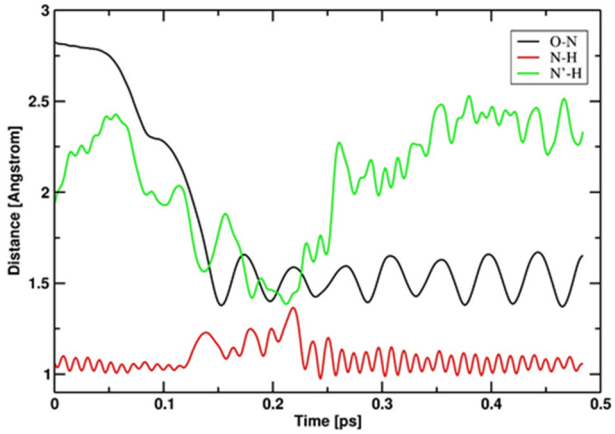

Figure 15. Sketch of the first and second reaction steps of ammonia with OH radicals. The most relevant bonding interactions deduced from Car–Parrinello simulations are highlighted. Color-code: blue—nitrogen, red—oxygen; white—hydrogen.

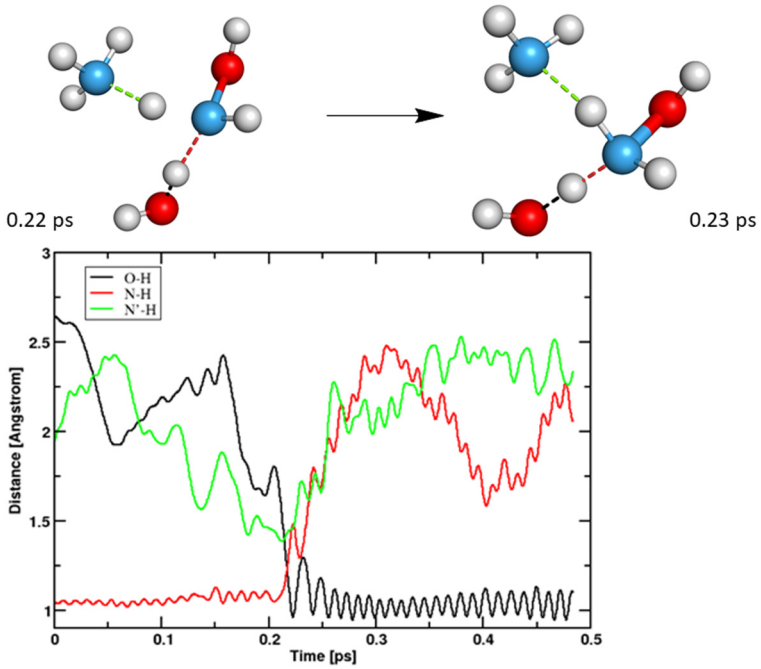

Figure 16. Sketch of the third and fourth reaction steps of ammonia with OH radical and NH_3 molecule. The most relevant bonding interactions deduced from Car–Parrinello simulations are highlighted. Color-code: blue—nitrogen, red—oxygen; white—hydrogen.

3.1.2. Cathodic Reactions

Under cathodic conditions, reactions with CO_2 in the solution were also observed. The most promising reaction which took place is the formation of formic acid, which is depicted in Figure 17.

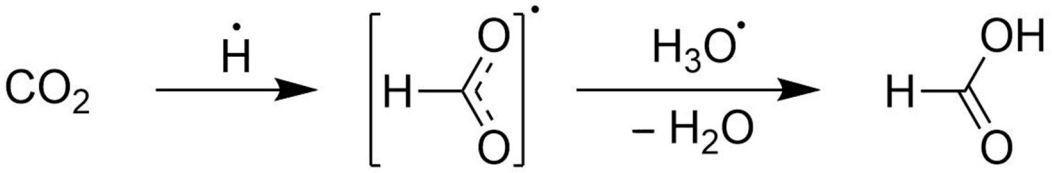

Figure 17. Elementary reaction steps that lead to the formation of an HCOOH molecule in system 2. The initial temperature was set to 300 K.

The first reaction step corresponds to the attack of hydrogen radical on carbon in CO_2, which results in the formation of an HCOO radical after 0.05 ps of simulation and the formation of the H-C bond. The second reaction step is the hydrogen radical transfer from an H_3O radical to the formerly formed intermediate yielding closed-shell formic acid after 0.32 ps of simulation. Key bond lengths for the first and second reaction steps are depicted in Figures 18 and 19.

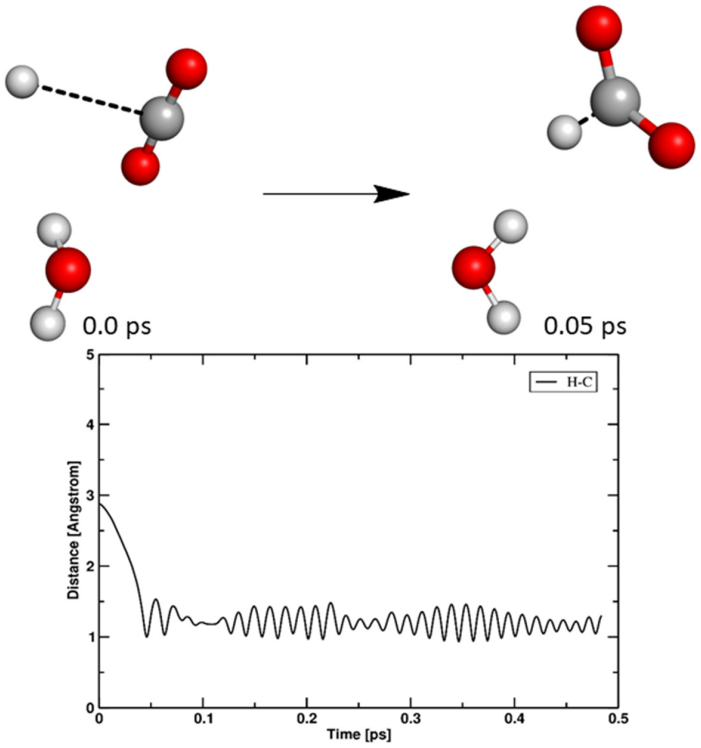

Figure 18. Sketch of the single reaction step of hydrogen radical reaction with carbon dioxide. The relevant bonding interaction deduced from Car–Parrinello simulations is highlighted. Color-code: red—oxygen; black—carbon; white—hydrogen.

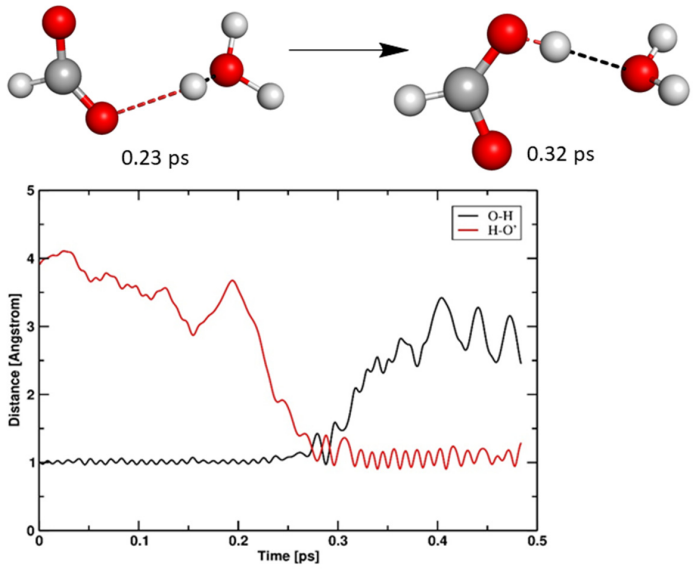

Figure 19. Sketch of the first and second reaction steps of the reaction of hydrogen radical with carbon dioxide. The most relevant bonding interactions deduced from Car–Parrinello simulations is highlighted. Color-code: red—oxygen; black—carbon; white—hydrogen.

3.2. Ethanimine and Carbon Dioxide in Aqueous Solution

3.2.1. Anodic Reactions

Additionally, the reactions of ethanimine under electrolytic conditions in systems 3 and 4 are under investigation. The chemically most interesting reactions took place under anodic properties, that is, with the participation of OH radicals. The first two reactions observed led to the formation of the stable zwitter-ionic species nitrosoethane, shown in Figure 20.

The first reaction step of mechanism 1 corresponds to the attack of a hydroxyl radical on the nitrogen atom of ethanimine, which results in the formation of an RNHOH radical after 0.09 ps of simulation. The formed reactive intermediate is attacked further by a second OH radical within 0.02 ps. As a result, a stable closed-shell zwitter-ionic species is formed. Key bond lengths for the first and second reaction steps are depicted in Figure 21. The process of zwitter-ion formation takes 0.27 ps in the Car–Parrinello MD simulation.

The single reaction step shown in Figure 22 corresponds to the hydrogen radical transfer between the unstable open-shell intermediate, the formation mechanism of which was part of the reaction shown in Figure 20, and a second ethanimine molecule.

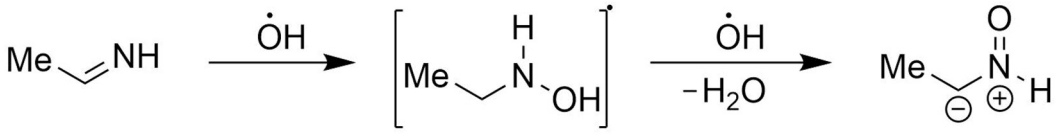

Figure 20. Sequence of elementary reaction steps that lead to the formation of the RHNO molecule in system 3. The initial temperature was set to 250 K.

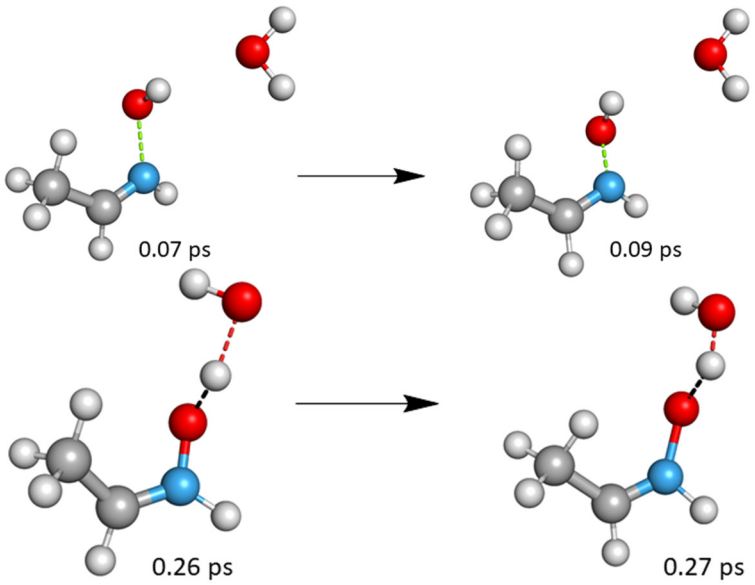

Figure 21. *Cont.*

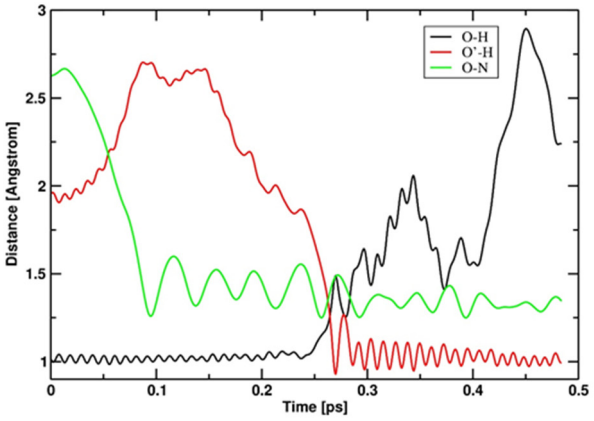

Figure 21. Sketch of the first and second reaction steps of ethanimine with OH radicals. The most relevant bonding interactions deduced from Car–Parrinello simulations are highlighted. Color-code: blue—nitrogen, red—oxygen; white—hydrogen.

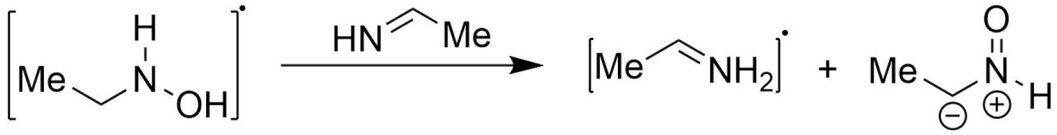

Figure 22. Sequence of elementary reaction steps that lead to the formation of zwitter-ion in system 3. The initial temperature of the system was set to 250 K.

The reaction yields the zwitter-ionic closed-shell species and an ethylamine radical after 0.25 ps of simulation. Key bond lengths for the single reaction step are depicted in Figure 23.

Furthermore, the formation of (E)-acetaldehydeoxime has been observed during the simulation, which is depiceted in Figure 24.

There are two different possible mechanism for this reaction, which are shown in Figures 23 and 25. The first reaction starts with the attack of a hydroxyl radical on the nitrogen atom of ethanimine, and this results in the formation of an RNHOH radical after 0.08 ps of simulation. The formed reactive intermediate is attacked further by a second OH radical within 0.01 ps, so the reaction is completed within 0.11 ps. As a result, two stable closed-shell species are formed: oxime and water. Key bond lengths for the first and second reaction steps are depicted in Figure 25.

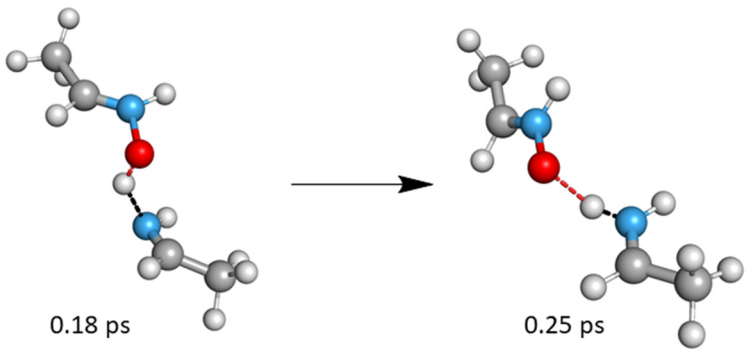

Figure 23. *Cont.*

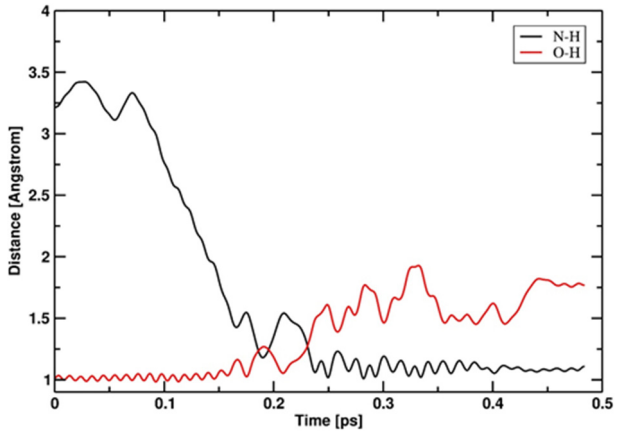

Figure 23. Sketch of the reactive open shell intermediate with another ethanimine molecule, leading to the zwitter-ion and an ethanimine radical. Color-code: blue—nitrogen, red—oxygen; white—hydrogen.

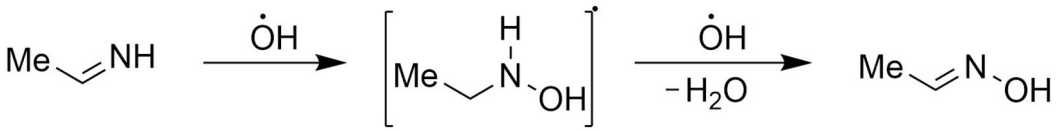

Figure 24. Sequence of elementary reaction steps that lead to the formation of an oxime molecule in system 4. The initial temperature of the system was set to 250 K.

Not only the formation of the (E)-isomer of acetaldehydeoxime can be observed, but also the formation of (Z)-acetaldehydoxime, which is depicted in Figure 26.

In the second reaction the first step corresponds to the hydrogen radical abstraction by hydroxyl radical after 0.05 ps of simulation. The first step is completed after 0.01 ps and yields a nitrene radical. The second step is represented by the addition of a second hydroxyl radical to the previously formed open-shell intermediate. The reaction is completed after 0.36 ps of simulation. Key bond lengths for the first and second reaction steps are depicted in Figure 27.

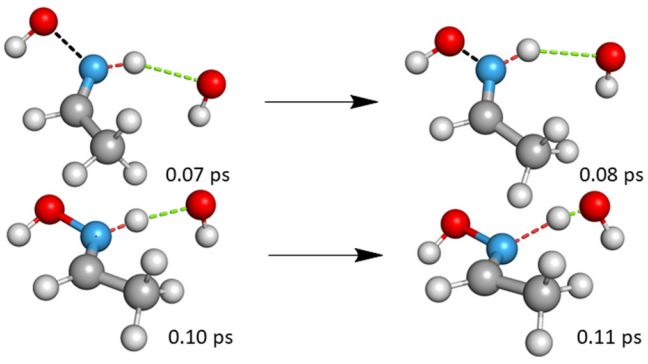

Figure 25. *Cont.*

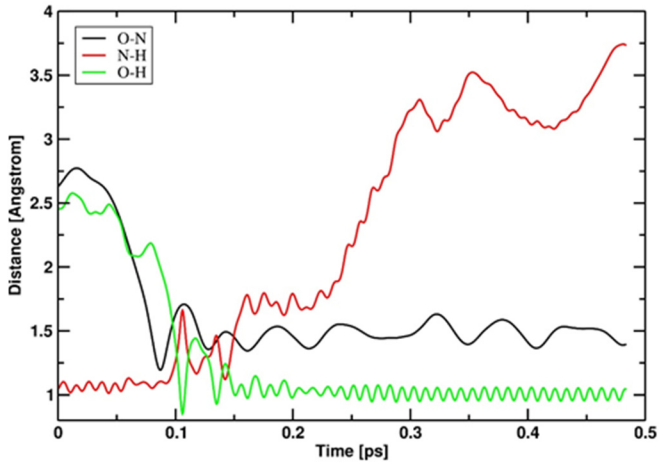

Figure 25. Sketch of the two reaction steps taking place. In the first step the reactive intermediate is formed via attack of the first hydrogen radical. In the second step the intermediate radical is attacked by the second OH-radical. Elimination of water leads to the formation of the closed-shell oxime molecule. Color-code: blue—nitrogen, red—oxygen; white—hydrogen.

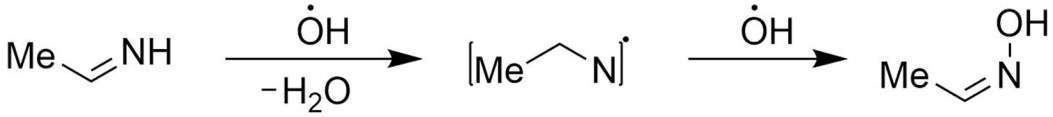

Figure 26. Sequence of elementary reaction steps that lead to the formation of an oxime molecule in system 4. The initial temperature of the system was set to 250 K.

3.2.2. Cathodic Reactions

In another reaction taking place, an imine molecule is attacking a CO_2 molecule under cathodic conditions. The product of the reaction is the radical and zwitter-ionic species of a carbamic acid derivative. The mechanism of the reaction is depicted in Figure 28.

Its first reaction step corresponds to the hydrogen radical abstraction by a free hydrogen radical after 0.04 ps of simulation. The first step is completed after 0.01 ps and yields an imine radical. The second step is represented by the addition of the previously formed reactive open-shell intermediate to carbon dioxide molecule, so a new C-N σ-bond was formed.

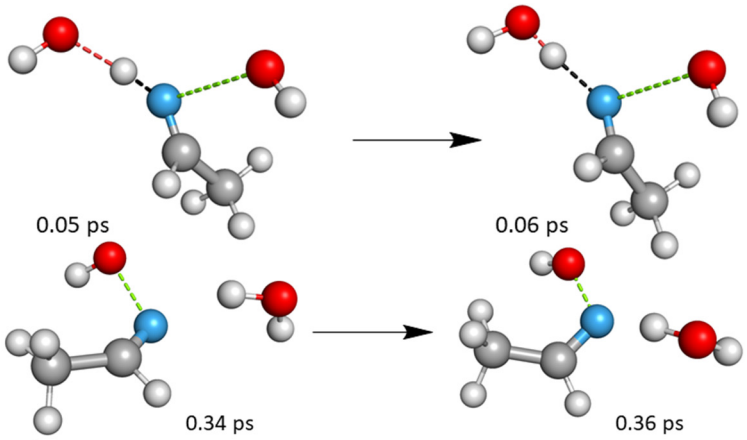

Figure 27. *Cont.*

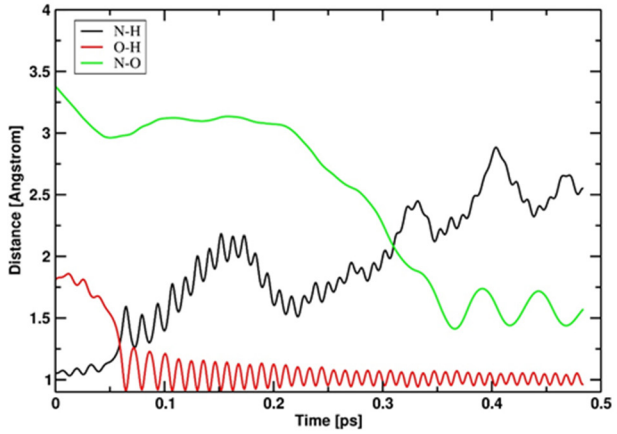

Figure 27. Sketch of the two reaction steps taking place. The first step shows the attack of an OH radical on the ethanimine molecule and the elimination of water. This reaction leads to the formation of a reactive nitrene radical which is attacked by another OH radical in the second step, forming the closed-shell oxime. Color-code: blue—nitrogen, red—oxygen; white—hydrogen.

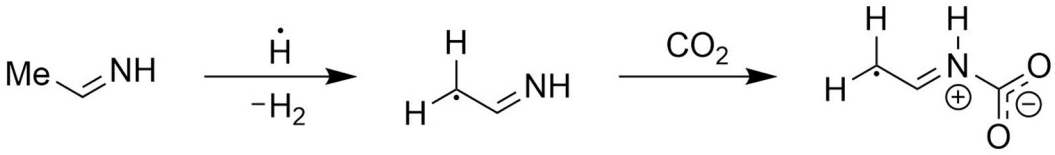

Figure 28. Sequence of elementary reaction steps that lead to the formation of zwitter-ion radical in system 4. The initial temperature of the system was set to 250 K.

Key bond lengths for the first and second reaction steps are depicted in Figure 29.

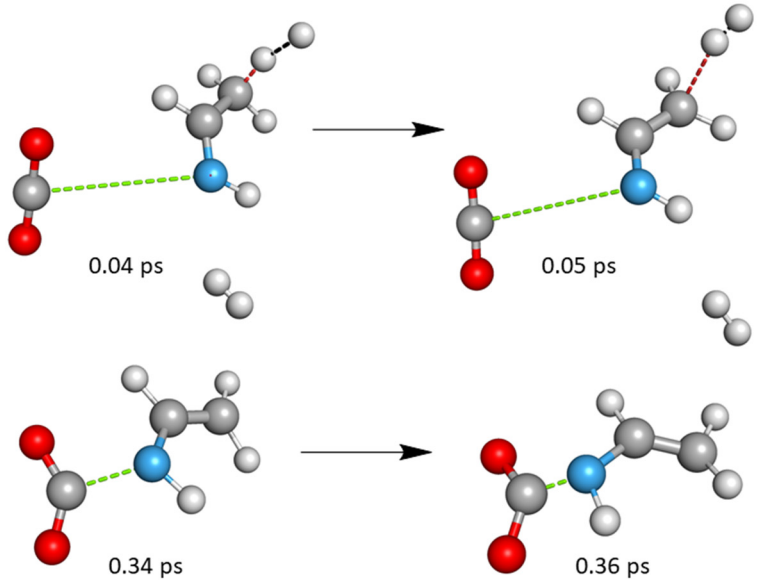

Figure 29. *Cont.*

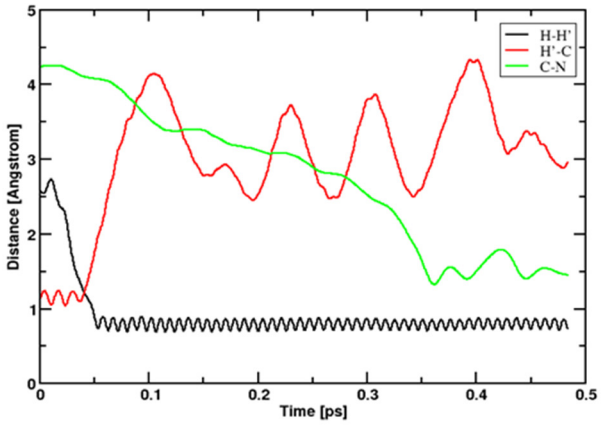

Figure 29. Sketch of the two reactions taking place. In the first step the elimination of hydrogen after the attack of a hydrogen radical is shown, leading to a reactive open shell intermediate. The second step corresponds to the attack of a carbon dioxide on the prior formed ethanimine radical leading to a carbamic acid-like radical. Color-code: blue—nitrogen, red—oxygen; white—hydrogen.

3.3. Energetics

The electronic energies and enthalpies of formation were calculated using various methods in Gaussian 16 as stated in the method section. The complete results are to be found in the Supplementary Materials. For comparison, experimental data from literature are provided. From these electronic energies and enthalpies of formation the energies for the corresponding reactions were calculated. The results are shown in Tables 1 and 2 for comparison of methods. The best results are provided using the BLYP-D3 functional, certainly a fortuitous agreement. It shows the lowest deviation values from the experimental data. Second best results are given by the Møller–Plesset perturbation method, MP2. The B2PLYP-D3 double-hybrid functional and the B3LYP hybrid functional yield comparable results. Comparable results to the previously mentioned hybrid functionals are provided by the CCSD functional with the aug-cc-pVTZ basis set. The coupled cluster CCSD method with a small basis set provides higher deviations from the experimental data. In contrast to the basis set, the use of an implicit solvent hardly affects the results. Finally, the worst results are obtained by the Hartree–Fock method, the deviations are in the order of magnitude of the reaction enthalpies.

Table 1. Deviation of the reaction enthalpies $\Delta_r H$ calculated with Gaussian 16 in comparison to the experimental values.

Reaction	$\Delta_r H$ (exptl)/kcal · mol^{-1}	Source	Deviation (theo-exptl)/kcal · mol^{-1}						
			BLYP	B3LYP	B2PLYP	HF	MP2	CCSD	CCSD/aug
4 ·OH + NH_3 → HNO + 3 H_2O	−175.90	NIST [35]	7.86	18.81	16.41	110.71	1.36	25.25	18.19
2 NH_3 + 4 ·OH → NO· + NH_4 + 3 H_2O	−124.27	NIST [35], ACTC [36,37]	7.91	22.36	20.99	109.99	15.59	35.70	20.16
NH_3 + 2 ·OH → NH_2OH + H_2O	−75.86	NIST [35], ACTC [36,37]	1.44	6.55	6.91	55.78	1.90	13.04	8.86
2 NH_3 + 3 ·OH → HNO + NH_4 + 2 H_2O	−54.93	NIST [35], ACTC [36,37]	5.73	19.71	20.22	97.45	14.91	32.52	18.24
2 ·OH + imin → H_2O + imOH	−87.56	NIST [35], ACTC [36,37]	−2.22	3.64	3.90	56.48	−1.26	11.22	-

Table 2. The deviation of the inner reaction energies $\Delta_r E$ calculated with Gaussian 16 from the experimental reaction enthalpies ΔH_r.

Reaction	$\Delta_r H$ (exptl)/kcal · mol^{-1}		Deviation ($\Delta_r E$(theo) − ΔH_r(exptl))/kcal · mol^{-1}						
			BLYP	B3LYP	B2PLYP	HF	MP2	CCSD	CCSD/aug
4 ·OH + NH_3 → HNO + 3 H_2O	−175.90	NIST [35]	3.29	13.78	11.02	104.60	−3.50	19.80	12.99
2 NH_3 + 4 ·OH → NO· + NH_4 + 3 H_2O	−124.27	NIST [35], ACTC [36,37]	8.40	22.32	20.14	110.56	9.10	32.73	14.65
NH_3 + 2 ·OH → NH_2OH + H_2O	−75.86	NIST [35], ACTC [36,37]	−3.08	1.63	1.81	49.90	−3.07	7.79	3.75
2 NH_3 + 3 ·OH → HNO + NH_4 + 2 H_2O	−54.93	NIST [35], ACTC [36,37]	8.42	21.72	21.51	99.72	12.61	31.49	14.58
2 ·OH + imin → H_2O + imOH	−87.56	NIST [35], ACTC [36,37]	−11.53	−5.91	−5.74	46.42	−10.71	1.48	-

4. Conclusions

The electrolytic reactions of ammonia and ethanimine in a carbon dioxide enriched aquatic solution were investigated by the use of Car–Parrinello molecular dynamics. A variety of reaction mechanisms and products was determined. In the considered timescale of 0.5 ps, the formation of both open- and closed-shell products was observed, among the most important being consecutive products of hydroxylamine and formic acid. At this point, it should be emphasized that our approach with many reactive species overestimates reactions that demand the simultaneous attack of two reactive species. An example is the NH_2OH formation where the two reaction steps are nearly simultaneous. Additionally, our picture is not complete in the sense that we cannot perform a sufficient number of simulation runs to observe all the reactions that are possible in a system.

While we found a variety of reaction pathways, there are some characteristic patterns. Under anodic conditions, typically the first reaction step is a simple hydrogen abstraction by OH radicals. In the case of ammonia this attack is sometimes almost simultaneous with the formation of an N-O bond corresponding to a radical recombination. Similarly, water and hydroxylamine are formed. Further simple abstractions of hydrogen by OH radicals lead to products like HNO. Under cathodic conditions the formation of molecular hydrogen is predominant. Additionally, we observed the addition of nascent hydrogen at the carbon atom of CO_2. In the case of ethanimine two initial reactions predominate under anodic conditions: the attachment of OH radicals to the nitrogen atoms and the abstraction of the hydrogen atom bound to nitrogen. Under cathodic conditions it is one of the hydrogen atoms of the methyl group which is abstracted by an OH radical. We observe interesting further steps involving CO_2.

How does this compare to the experiment? In contrast to the experiment [16–18], we observe predominantly the formation of an N-O bond, but we never observe the formation of an N-N bond, even if we use high ammonia concentrations. This supports the mechanism assumed on the basis of experimental data, where the formation of N-N bonds is postulated to be, at least in part, an effect of surface catalysis. Experimentally, NH_2OH and consecutive products are obtained at high voltages.

The energetic calculations that were performed show that all reactions observed are energetically favored in good agreement with experimental data. The best values in comparison to the experimental heats of formation are obtained using the BLYP-D3-functional and the MP2 method. Under the aspect of "power to chemicals", it is interesting to note that the formation of formic acid and a carbamic acid species from CO_2 were observed. It is an interesting finding that CO_2 can be converted into formic acid without a

particular surface catalysis. The cathodic formation of molecular hydrogen is, of course, interesting under the aspect of "power to fuel". For the decontamination of wastewater via the degradation of harmful substances, further investigation is necessary. Even if we started from a relatively simple model (no electrolyte, no electrodes) a large number of intermediates and products were observed. In view of the renewed interest in electrolysis experiments, it makes sense to systematically enter this vast field stepwise from a theoretical side, starting with systems that are as simple as possible.

Supplementary Materials: The following are available online at https://www.mdpi.com/article/10.3390/en14206510/s1.

Author Contributions: Methodology, software, visualization, data curation and writing—review and editing, I.G.; data curation, visualization and writing—original draft preparation, L.S.; conceptualization, methodology, validation, writing—review and editing, project administration and funding acquisition, I.F. All authors have read and agreed to the published version of the manuscript.

Funding: The study was supported by the Deutsche Forschungsgemeinschaft (DFG), grant FR1246/10-1.

Acknowledgments: Part of the calculations was performed on the local cluster of the Leibniz University Hannover at the Leibniz University IT services.

Conflicts of Interest: The authors declare no conflict of interest.

References

1. Bismo, S.; Irawan, K.; Karamah, E.F.; Saksono, N. On the Production of OH Radical through Plasma Electrolysis Mechanism for the Processing of Ammonia Waste Water. *J. Chem. Chem. Eng.* **2013**, *7*, 6.
2. Peters, M.; Köhler, B.; Kuckshinrichs, W.; Leitner, W.; Markewitz, P.; Müller, T.E. Chemical technologies for exploiting and recycling carbon dioxide into the value chain. *ChemSusChem* **2011**, *4*, 1216–1240. [CrossRef]
3. Martín, A.J.; Larrazábal, G.O.; Pérez-Ramírez, J. Towards sustainable fuels and chemicals through the electrochemical reduction of CO_2: Lessons from water electrolysis. *Green Chem.* **2015**, *17*, 5114–5130. [CrossRef]
4. Sternberg, A.; Bardow, A. Power-to-What?—Environmental assessment of energy storage systems. *Energy Environ. Sci.* **2015**, *8*, 389–400. [CrossRef]
5. Patterson, T.; Savvas, S.; Chong, A.; Law, I.; Dinsdale, R.; Esteves, S. Integration of Power to Methane in a waste water treatment plant–A feasibility study. *Bioresour. Technol.* **2017**, *245*, 1049–1057. [CrossRef] [PubMed]
6. Mebrahtu, C.; Nohl, M.; Dittrich, L.; Foit, S.R.; de Haart, L.B.; Eichel, R.A.; Palkovits, R. Integrated Co-Electrolysis and Syngas Methanation for the Direct Production of Synthetic Natural Gas from CO_2 and H_2O. *ChemSusChem* **2021**, *14*, 2295. [CrossRef] [PubMed]
7. O'Shea, R.; Wall, D.M.; McDonagh, S.; Murphy, J.D. The potential of power to gas to provide green gas utilising existing CO_2 sources from industries, distilleries and wastewater treatment facilities. *Renew. Energy* **2017**, *114*, 1090–1100. [CrossRef]
8. Thema, M.; Bauer, F.; Sterner, M. Power-to-Gas: Electrolysis and methanation status review. *Renew. Sustain. Energy Rev.* **2019**, *112*, 775–787. [CrossRef]
9. Klüh, D.; Waldmüller, W.; Gaderer, M. Kolbe Electrolysis for the Conversion of Carboxylic Acids to Valuable Products—A Process Design Study. *Clean Technol.* **2021**, *3*, 1–18. [CrossRef]
10. Kotowicz, J.; Węcel, D.; Brzęczek, M. Analysis of the work of a "renewable" methanol production installation based ON H2 from electrolysis and CO_2 from power plants. *Energy* **2021**, *221*, 119538. [CrossRef]
11. Albert, J.; Jess, A.; Kern, C.; Pöhlmann, F.; Glowienka, K.; Wasserscheid, P. formic acid-based fischer–tropsch synthesis for green fuel production from wet waste biomass and renewable excess energy. *ACS Sustain. Chem. Eng.* **2016**, *4*, 5078–5086. [CrossRef]
12. Kreitz, B.; Brauns, J.; Wehinger, G.D.; Turek, T. Modeling the Dynamic Power-to-Gas Process: Coupling Electrolysis with CO_2 Methanation. *Chem. Ing. Tech.* **2020**, *92*, 1992–1997. [CrossRef]
13. Lu, X.; Musin, R.N.; Lin, M.C. Gas-phase reactions of HONO with HNO and NH3: An ab initio MO/TST study. *J. Phys. Chem. A* **2000**, *104*, 5141–5148. [CrossRef]
14. Frank, I. Ab-Initio Molecular Dynamics Simulation of the Electrolysis of Waste Water. *ChemistrySelect* **2019**, *4*, 4376–4381. [CrossRef]
15. Kiakojouri, A.; Nadimi, E.; Frank, I. Ab-Initio Molecular Dynamics Simulation of Condensed-Phase Reactivity: The Electrolysis of Amino Acids and Peptides. *Molecules* **2020**, *25*, 5415. [CrossRef] [PubMed]
16. Oswin, H.G.; Salomon, M. The anodic oxidation of ammonia at platinum black electrodes in aqueous KOH electrolyte. *Can. J. Chem.* **1963**, *41*, 1686–1694. [CrossRef]
17. Despić, A.R.; Dražić, D.M.; Rakin, P.M. Kinetics of electrochemical oxidation of ammonia in alkaline solution. *Electrochim. Acta* **1966**, *11*, 997–1005. [CrossRef]
18. Bunce, N.J.; Bejan, D. Mechanism of electrochemical oxidation of ammonia. *Electrochim. Acta* **2011**, *56*, 8085–8093. [CrossRef]

19. Blumberger, J.; Bernasconi, L.; Tavernelli, I.; Vuilleumier, R.; Sprik, M. Electronic structure and solvation of copper and silver ions: A theoretical picture of a model aqueous redox reaction. *J. Am. Chem. Soc.* **2004**, *126*, 3928–3938. [CrossRef]
20. Zhang, C.; Sayer, T.; Hutter, J.; Sprik, M. Modelling electrochemical systems with finite field molecular dynamics. *J. Phys. Energy* **2020**, *2*, 032005. [CrossRef]
21. Vassilev, P.; Louwerse, M.J.; Baerends, E.J. Ab initio molecular dynamics simulation of the OH radical in liquid water. *Chem. Phys. Lett.* **2004**, *398*, 212–216. [CrossRef]
22. Marx, D.; Hutter, J. *Ab Initio Molecular Dynamics: Basic Theory and Advanced Methods*; Cambridge University Press: Cambridge, UK, 2009.
23. Car, R.; Parrinello, M. Unified approach for molecular dynamics and density-functional theory. *Phys. Rev. Lett.* **1985**, *55*, 2471. [CrossRef]
24. Hofbauer, F.; Frank, I. CPMD simulation of a bimolecular chemical reaction: Nucleophilic attack of a disulfide bond under mechanical stress. *Chem. A Eur. J.* **2012**, *18*, 16332–16338. [CrossRef]
25. CPMD. Copyright IBM Corp, 1990–2008, Copyright MPI für Festkörperforschung Stuttgart 1997–2001. Available online: http://www.cpmd.org/ (accessed on 4 October 2021).
26. Frank, I. Chemische Reaktionen "on the fly". *Angew. Chem.* **2003**, *115*, 1607–1609. [CrossRef]
27. Becke, A.D. Density-functional exchange-energy approximation with correct asymptotic behavior. *Phys. Rev. A* **1988**, *38*, 3098. [CrossRef]
28. Lee, C.; Yang, W.; Parr, R.G. Development of the Colle-Salvetti correlation-energy formula into a functional of the electron density. *Phys. Rev.* **1988**, *37*, 785. [CrossRef]
29. Grimme, S. Semiempirical GGA-type density functional constructed with a long-range dispersion correction. *J. Comput. Chem.* **2006**, *27*, 1787–1799. [CrossRef]
30. Frisch, M.J.; Trucks, G.W.; Schlegel, H.B.; Scuseria, G.E.; Robb, M.A.; Cheeseman, J.R.; Scalmani, G.; Barone, V.; Petersson, G.A.; Nakatsuji, H.; et al. *Gaussian 16 Rev. C.01*; Gaussian Inc.: Wallingford, CT, USA, 2016.
31. Troullier, N.; Martins, J.L. Efficient pseudopotentials for plane-wave calculations. *Phys. Rev. B* **1991**, *43*, 1993. [CrossRef] [PubMed]
32. Boero, M.; Parrinello, M.; Terakura, K.; Weiss, H. Car—Parrinello study of Ziegler—Natta heterogeneous catalysis: Stability and destabilization problems of the active site models. *Mol. Phys.* **2002**, *100*, 2935–2940. [CrossRef]
33. Zahn, S.; MacFarlane, D.R.; Izgorodina, E.I. Assessment of Kohn–Sham density functional theory and Møller–Plesset perturbation theory for ionic liquids. *Phys. Chem. Chem. Phys.* **2013**, *15*, 13664–13675. [CrossRef] [PubMed]
34. Gunnarsson, O.; Lundqvist, B.I. Exchange and correlation in atoms, molecules, and solids by the spin-density-functional formalism. *Phys. Rev. B* **1976**, *13*, 4274. [CrossRef]
35. Becke, A.D. Density-functional thermochemistry. III. The role of exact exchange. *J. Chem. Phys.* **1993**, *98*, 5648. [CrossRef]
36. Grimme, S. Semiempirical hybrid density functional with perturbative second-order correlation. *J. Chem. Phys.* **2006**, *124*, 034108. [CrossRef]
37. Møller, C.; Plesset, S.M. Note on an approximation treatment for many-electron systems. *Phys. Rev.* **1934**, *46*, 618. [CrossRef]
38. Wiberg, K.B. *Ab Initio Molecular Orbital Theory*; Hehre, W.J., Radom, L., Schleyer, P.V.R., Pople, J.A., Eds.; John Wiley: New York, NY, USA, 1986; 548p. [CrossRef]
39. Miertuš, S.; Scrocco, E.; Tomasi, J. Electrostatic interaction of a solute with a continuum. A direct utilizaion of AB initio molecular potentials for the prevision of solvent effects. *Chem. Phys.* **1981**, *55*, 117–129. [CrossRef]
40. Chase, M.W., Jr. *NIST-JANAF Thermochemical Tables, Monograph 9, Part 1*; American Institute of Physics: New York, NY, USA, 1998. Available online: https://www.nist.gov/ (accessed on 4 October 2021).
41. Ruscic, B.; Pinzon, R.E.; Von Laszewski, G.; Kodeboyina, D.; Burcat, A.; Leahy, D.; Montoy, D.; Wagner, A.F. Active Thermochemical Tables: Thermochemistry for the 21st century. In *Proceedings of the SciDAC 2005, SCIENTIFIC DISCOVERY THROUGH ADVANCED COMPUTING, San Francisco, CA, USA, 26–30 June 2005*; IOP Publishing: Bristol, UK; Volume 16, p. 078.
42. Ruscic, B.; Pinzon, R.E.; Morton, M.L.; von Laszevski, G.; Bittner, S.J.; Nijsure, S.G.; Amin, K.A.; Minkoff, M.; Wagner, A.F. Introduction to active thermochemical tables: Several "key" enthalpies of formation revisited. *J. Phys. Chem. A* **2004**, *108*, 9979–9997. [CrossRef]